High-pass negative group delay analysis of single capacitor three-port circuit

Nour Mohammad Murad, Antonio Jaomiary, Samar Yazdani, Fayrouz Haddad, Mathieu Guerin, George Chan, Wenceslas Rahajandraibe, Sahbi Baccar

High-pass negative group delay analysis of single capacitor three-port circuit

Nour Mohammad Murad, Antonio Jaomiary, Samar Yazdani, Fayrouz Haddad, Mathieu Guerin, George Chan, Wenceslas Rahajandraibe, Sahbi Baccar

Abstract: This paper develops high-pass (HP) negative group delay (NGD) investigation based on three-port lumped circuit. The main particularity of the proposed three-port passive topology is the consideration of only a single element represented by a capacitor. The S-matrix equivalent model of the three-port circuit topology is established from the admittance matrix approach. The frequency-dependent basic expressions are considered in order to make the HP-NGD analysis. Then, the existence condition of HP-NGD function type is analytically demonstrated. The specific characteristics and synthesis equations of HP-NGD circuit with respect to the desired optimal NGD value are established. The validity of the HP-NGD theory is verified by a prototype of three-port circuit. The proof-of-concept (POC) single capacitor based three-port circuit presents an NGD response and characteristics from analytical calculation and simulation in very good correlation.

Keywords: Circuit theory, high-pass (HP) negative group delay (NGD), NGD passive circuit, HP-NGD analysis, NGD specifications, three-port topology.

Acknowledgements: The authors address a grateful thank to Prof. Blaise Ravelo for his scientific help about the NGD analysis and the NGD development in the manuscript.

1. INTRODUCTION

The unfamiliar negative group delay (NGD) function is expected to be useful to improve the imperfection of communication front-end systems by means of delay compensation [1-2], and frequency independent phase shifter design [3-4]. Other applications of NGD function concern the antenna array design [5] and signal distortion correction by reducing the delay effect [6-8]. The development of NGD function application depends on its development and also the open understanding to the non-specialist electronic engineers.

At the beginning of the research work on this intriguing topic, curious questions were wondered about the existence of NGD phenomenon. The NGD effect was firstly experimented with optical systems [9-12]. The NGD optical experimental setup depends on the use of negative group velocity (NGV) media [10]. The NGD pulse propagation was found in the photonic crystal structure [11]. However, the NGD effect was also generated with two pulse interference technique [12].

The existence and the diversity of NGD effect generator becomes an attractive topic for few electronic engineering researchers from 1990s to now [13-43]. It was found that the NGD effect can be interpreted in the time-domain by smoothed pulse signals with output propagating in time-advance compared to the input [13-17]. It was experimentally demonstrated with optical and electronic circuits that the NGD effect can appear with superluminality [12,16-17]. Nevertheless, it should be emphasized that the NGD effect does not contradict the causality principle because the instantaneous output is still spontaneously generated by the input [13-14]. After the time domain demonstration of the NGD effect with low-frequency (LF) circuits, radio frequency (RF) and microwave passive circuits exhibiting NGD effect were designed and tested [18-24]. The NGD passive circuits were remarkably explored in yearly 2000s by using metamaterial based artificial periodical transmission lines (TLs) [18-19]. Even several band NGD circuits using split ring resonator elements were also designed [20-21]. However, to generate significant NGD values, microstrip circuit constituted by many periodical cells is necessary [18-20]. Therefore, the size and attenuation losses become excessively high. This critical limitation becomes an open challenge for microwave NGD circuit design researchers who are looking for low loss and compact NGD passive circuits during the two last decades [22-24]. To compensate losses, NGD active topologies were also proposed [25-27]. The microwave NGD active circuits [25-27] can be designed with distributed topologies in order to operate higher in frequencies. Behind the diversity of NGD structures [13-27], the meaning of NGD effect becomes difficult to interpret.

For this reason, an easy to understand and fundamental approach of NGD circuit investigation is necessary. In this way, an innovative fundamental NGD circuit theory inspired from the similitude with the filter theory was initiated [28-29]. Some elementary lumped topologies of NGD active circuits using field effect transistor (FET) combined with resistors, inductors and capacitors were identified [28]. Hence, simpler passive topologies of low-pass (LP) NGD [29-31], high-pass (HP) NGD [32-33], bandpass (BP) NGD [34-37] and even the very original stop-band (SB) NGD [38-39] lumped cells. Those identified NGD lumped topologies [29-40] are constituted by resistive-inductive (RL), resistive-capacitive (RC), inductive-capacitive (LC) and resistive-inductive-capacitive (RLC) networks were identified. The unfamiliar NGD passive circuits [28-34, 37-40] were generally designed with two-port topologies.

Then, very recent research work progress states the feasibility of NGD circuit designed based on three- [35-36,40-41] and four- [42-43] port topologies. We are particularly attracted to the design feasibility of fully capacitive topology as proposed in [36]. In the present paper, we are studying the modelling and designability of NGD three-port circuit constituted only by a single capacitor. The paper is organized in four sections as follows:

- Section 2 is focused on the general theory of the three-port topology under study. The topological description is introduced. The S-matrix model in function of the single capacitor parameter value. The identification method HP-NGD aspect will be elaborated.
- Section 3 develops the NGD analysis and the synthesis formulation of the single capacitor parameter value in function of the desired NGD value.
- Section 4 will examine the validation results. A proof of concept (PoC) of single capacitor three-port circuit will be described. Comparison between computed results from analytical modelling and simulations will be discussed.
- Section 5 will present the conclusion.

2. S-MATRIX MODEL AND ANALYSIS OF THE THREE-PORT TOPOLOGY CONSTITUTED BY SINGLE CAPACITOR

This section introduces the circuit theory of three-port topology under study. The S-matrix model will be established by means of admittance matrix (Y-matrix). Then, analytical method for NGD function type identification is elaborated.

2.1. Block diagram representation of three-port topology

The topological description of the three-port topology can be performed by considering the voltage sources V_k with k={1,2,3} connected to port ①, port ② and port ③ like the approach developed in [35-36,40-43]. By taking s as Laplace variable, the analytical elaboration is defined by the 3-D vector of excitation voltage and the 3-D vector of induced access current [35-36,40-41]:

$$[V(s)] = \begin{bmatrix} V_1(s) \\ V_2(s) \\ V_3(s) \end{bmatrix} \quad (1)$$

$$[I(s)] = \begin{bmatrix} I_1(s) \\ I_2(s) \\ I_3(s) \end{bmatrix} \quad (2)$$

The ideal diagram can be drawn by the three-port black box of 3-D Y-matrix [Y(s)] introduced in Fig. 1.

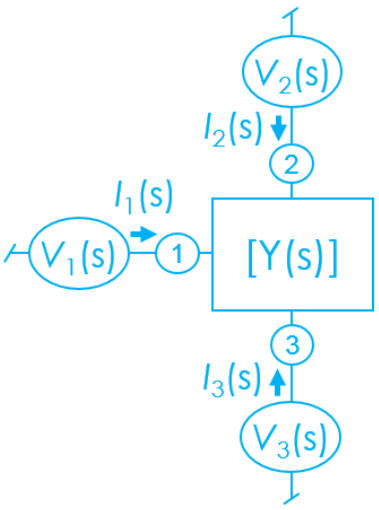

Figure 1: Y-matrix based diagram.

The generalized Ohm's law associated to the Y-matrix equivalent model represented by the diagram of Fig. 1 can be denoted by [35-36, 40-41]:

$$\begin{bmatrix} I_1(s) \\ I_2(s) \\ I_3(s) \end{bmatrix} = [Y(s)] \times \begin{bmatrix} V_1(s) \\ V_2(s) \\ V_3(s) \end{bmatrix} \tag{3}$$

with the Y-matrix:

$$[Y(s)] = \begin{bmatrix} Y_{11}(s) & Y_{12}(s) & Y_{13}(s) \\ Y_{21}(s) & Y_{22}(s) & Y_{23}(s) \\ Y_{31}(s) & Y_{32}(s) & Y_{33}(s) \end{bmatrix} \tag{4}$$

2.2. General topology with elementary impedance

Before the NGD type identification, we can consider the Tee-shaped circuit shown by Fig. 2. This topology is composed by:

- an impedance, $Z(s)$ connected to port ①,
- and by identical two resistances, R connected to the other ones, port ② and port ③.

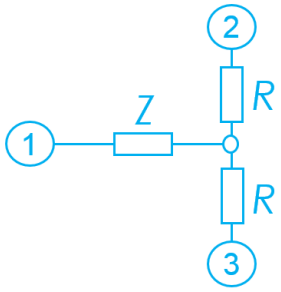

Figure 2: Three-port circuit constituted by resistor *R* and impedance *Z*.

The expression of Y-matrix associated to the considered three-port network can be determined from the Kirchhoff voltage law (KVL) and Kirchhoff current law (KCL). Accordingly, equation (4) can be rewritten as:

$$[Y(s)] = \frac{\begin{bmatrix} 2R & -R & -R \\ -R & R+Z(s) & -Z(s) \\ -R & -Z(s) & R+Z(s) \end{bmatrix}}{D_Y(s)} \tag{5}$$

with:

$$D_Y(s) = R[R+2Z(s)]. \tag{6}$$

The S-matrix equivalent model is derived from this Y-matrix expression in the next subsection.

2.3. S-matrix general model

The present S-matrix is established by considering the reference impedance R_0=50 Ω. According to the S-matrix theory, we have the Y-to-S matrix transform [35-36, 40-43]:

$$[S(s)] = \{[\Upsilon_4] - R_0[Y(s)]\} \times \{[\Upsilon_4] + R_0[Y(s)]\}^{-1} \tag{7}$$

with the 3-D identity matrix:

$$[\Upsilon_4] = \begin{bmatrix} 1 & 0 & 0 \\ 0 & 1 & 0 \\ 0 & 0 & 1 \end{bmatrix} \tag{8}$$

Substituting the Y-matrix given in equation (5) into matrix equation (7), we have the expression of S-matrix in function of *R* and *Z*:

$$[S(s)] = \begin{bmatrix} S_{11}(s) & S_{12}(s) & S_{13}(s) \\ S_{21}(s) & S_{22}(s) & S_{23}(s) \\ S_{31}(s) & S_{32}(s) & S_{33}(s) \end{bmatrix} \tag{9}$$

where the reflection coefficients are:

$$S_{11}(s) = \frac{(R+R_0)[R-R_0+2Z(s)]}{D_S(s)} \tag{10}$$

$$S_{22}(s) = S_{33}(s) = \frac{(R - R_0)(R + R_0) + 2R\left[R_0 + Z(s)\right]}{D_S(s)} \tag{11}$$

and the transmission coefficients are:

$$S_{12}(s) = S_{21}(s) = S_{31}(s) = S_{13}(s) = \frac{2R_0(R + R_0)}{D_S(s)} \tag{12}$$

$$S_{23}(s) = S_{32}(s) = \frac{2R_0\left[R_0 + Z(s)\right]}{D_S(s)} \tag{13}$$

where:

$$D_S(s) = (R + R_0)\left[R\ + 3R_0 + 2Z(s)\right] \tag{14}$$

2.4. Single component-based S-matrix simplified model of three-port topology

As objective of the present study, the NGD topology must be composed of at least a reactive component [31]. Accordingly, we can choose the impedance Z as a first order element. By the reason of simplicity, let us take R=0. Therefore, the reflection coefficient elements written in equation (6) is reduced as:

$$S_{11}(s) = \frac{2Z(s) - R_0}{3R_0 + 2Z(s)} \tag{15}$$

$$S_{22}(s) = S_{33}(s) = \frac{-R_0}{3R_0 + 2Z(s)}. \tag{16}$$

and the transmission coefficients:

$$S_{12}(s) = S_{21}(s) = S_{31}(s) = S_{13}(s) = \frac{2R_0}{3R_0 + 2Z(s)} \tag{17}$$

$$S_{23}(s) = S_{32}(s) = \frac{2\left[R_0 + Z(s)\right]}{3R_0 + 2Z(s)} \tag{18}$$

From this S-matrix, we must study the identification of the NGD function type of the proposed three-port topology by choosing the appropriate reactive component representing Z.

2.5. Recall on basic definition for NGD analysis

We remind that the NGD analysis [13-39] depends essentially on the elaboration of the transmission coefficient, $S_{mn}(s)$, with integer subscript, $m \neq n$. By taking the Laplace variable versus angular frequency, $s = j\omega$, with angular frequency ω, the transmission coefficient can be expressed as:

$$T(j\omega) = S_{mn}(j\omega) \tag{19}$$

The basic elements to be explored to pursue the NGD analysis are transmittance, $T(\omega)$, and phase, $\varphi(\omega)$ which are given by respectively:

$$T(\omega) = |T(j\omega)| \tag{20}$$

$$\varphi(\omega) = \arg[T(j\omega)] \tag{21}$$

This last expression can be derived according to the circuit theory associated GD defined by the following equation:

$$GD(\omega) = -\frac{\partial\varphi(\omega)}{\partial\omega} \tag{22}$$

The GD at very LF is given by:

$$GD_0 = GD(\omega \approx 0) \tag{23}$$

If GD_0<0, the circuit can be classified as LP-NGD topology with cut-off frequency as the root of equation:

$$GD(\omega) = 0\,. \tag{24}$$

The basic characteristics of this response are introduced as described in the following paragraph.

2.6. NGD function type identification

As a simple reactive element, we propose in the present study to choose the impedance as a capacitor *C*. Meanwhile, we have:

$$Z(s) = \frac{1}{C\,s}\,. \tag{25}$$

Fig. 3 represents the schematic of the simplified topology with a single capacitor connected to port ①. Port ② and port ③ are short-circuited.

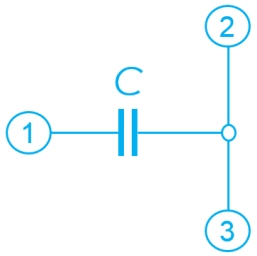

Figure 3: Three-port topology with single capacitor.

For this single capacitor three-port circuit, we have the reflection coefficients:

$$S_{11}(s) = \frac{2 - R_0 Cs}{2 + 3R_0 Cs} \tag{26}$$

$$S_{22}(s) = S_{33}(s) = \frac{-R_0 Cs}{2 + 3R_0 Cs} \tag{27}$$

and the transmission coefficients:

$$S_{12}(s) = S_{21}(s) = S_{13}(s) = S_{31}(s) = \frac{2R_0 Cs}{2 + 3R_0 Cs} \tag{28}$$

$$S_{23}(s) = S_{32}(s) = \frac{2(1+R_0Cs)}{2+3R_0Cs}. \quad (29)$$

We remind that the first order circuit canonical form of LP- or HP-NGD functions represented by a transmission coefficient can be written by [29-30]:

$$T(s) = T_0 \frac{1+a\,s}{1+b\,s} \quad (30)$$

where T_0, a and b are real coefficients. By identification of the transmission coefficients given by the before last two equations, we have the possibility to generate NGD function corresponding to transmission between port ② and port ③. The NGD characterization of the single capacitor three-port circuit shown in Fig. 3 will be elaborated by considering the transfer function from equation (29):

$$T(s) = S_{23}(s) = S_{32}(s). \quad (31)$$

Therefore, by identification, the parameters of canonical form proposed in equation (30) are expressed as:

$$\begin{cases} T_0 = 1 \\ a = R_0C \\ b = \dfrac{3R_0C}{2} \end{cases}. \quad (32)$$

We can remark that:

$$b = \frac{3a}{2}. \quad (33)$$

2.7. Frequency-dependent expressions of reflection coefficients, transmission coefficient and GD

By taking $s = j\omega$, the transmittance corresponding to relation (30) is expressed as:

$$T(j\omega) = \frac{1+j\omega\,a}{1+\dfrac{3j\omega\,a}{2}}. \quad (34)$$

The frequency-dependent transmission coefficient magnitude given in (20), with respect to following previous equation is given by:

$$T(\omega) = \frac{\sqrt{1+(\omega\,a)^2}}{\sqrt{1+\dfrac{9(\omega\,a)^2}{4}}}. \quad (35)$$

The corresponding phase response as defined by equation (21) is equal to:

$$\varphi(\omega) = \arctan(\omega\,a) - \arctan\left(\frac{3\omega\,a}{2}\right). \quad (36)$$

According to definition (22), the GD can be formulated as:

$$GD(\omega) = \frac{a(2-3a^2\omega^2)}{(a^2\omega^2+1)(9a^2\omega^2+4)}\,. \tag{37}$$

It is important to note also that the frequency-dependent reflection coefficient magnitudes with respect to equation (26) and equation (27) are given by:

$$S_{11}(\omega) = \frac{\sqrt{4+(\omega a)^2}}{\sqrt{4+9(\omega a)^2}} \tag{38}$$

$$S_{22}(\omega) = S_{33}(\omega) = \frac{\omega a}{\sqrt{4+9(\omega a)^2}}\,. \tag{39}$$

These expressions will serve to establish the NGD characterization in the following part of the paper.

2.8. Relationships between reflection coefficients, and GD versus transmission coefficient

By inverting the equation of transmission coefficient written in (35), we can determine the quantity (ωa) in function of *T*. Substituting the obtained expression:

- Into the reflection coefficient introduced in equation (38), we have the following relation:

$$S_{11} = \frac{\sqrt{8T^2-3}}{\sqrt{5}} \tag{40}$$

  We can understand that this relation works according to the range $1 \geq T \geq 2/3$ expected from equation (35).

- Into the other reflection coefficients introduced in equation (39), and thus, we have:

$$S_{22} = S_{33} = \frac{\sqrt{1-T^2}}{\sqrt{5}}\,. \tag{41}$$

  The previous relation is valid under condition $T \leq 1$ which is the normal case of passive circuit.

- Similarly, the same process applied to equation (37), we have the following expression:

$$GD(T) = \frac{a(3T^2-2)(9T^2-4)}{10T^2}\,. \tag{42}$$

We plot in Fig. 4(a), Fig. 4(b) and Fig. 4(c), these reflection coefficients and GD, respectively, by varying the transmission coefficient T from $T_{\min} = \sqrt{3/8}$ and $T_{\max} = 1$.

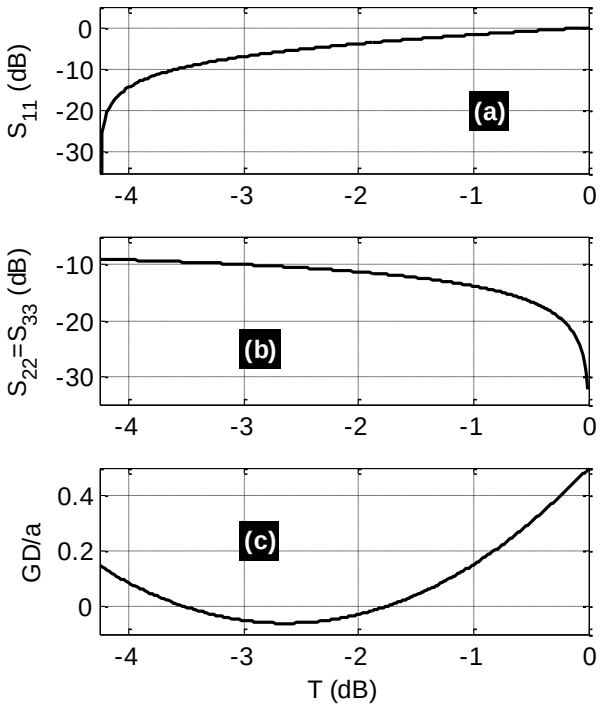

Figure 4: (a) S_{11}, (b) $S_{22}=S_{33}$ and (c) GD of the topology shown in Fig. 3 versus transmission coefficient.

3. HP-NGD ANALYSIS

This NGD analysis is aimed to establish the main analytical law of each parameter of the three-port topology under study.

3.1. Low frequency (LF) analysis

One of the most intuitive particular frequency enabling to perform the NGD analysis of any circuit is f=0 or very LFs. We can demonstrate that at this particular frequency, the S-parameters given by equation (35), equation (36) and equation (37) become:

$$\begin{cases} T(\omega \approx 0) = 1 \\ S_{11}(\omega \approx 0) = 1 \\ S_{22}(\omega \approx 0) = S_{33}(\omega \approx 0) = 1 \end{cases} . \tag{43}$$

Moreover, the GD defined by equation (23) can be written as:

$$GD_0 = \frac{a}{2} \tag{44}$$

We can remark that this quantity is always positive. This is one of the main conditions enabling to characterize an HP-NGD circuit.

3.2. NGD cut-off frequency

The positive root of equation (24) is equal to:

$$\omega_n = \frac{1}{a}\sqrt{\frac{2}{3}} \tag{45}$$

The sign of GD versus angular frequency is addressed in Table 1.

Angular frequency	$\omega < \omega_n$	$\omega = \omega_n$	$\omega > \omega_n$
sign[$GD(\omega)$]	$GD(\omega) > 0$	$GD(\omega) = 0$	$GD(\omega) < 0$

Table 1: Sign of GD

It can be understood as illustrated by Table 1 that the GD is always negative when $\omega > \omega_n$. Moreover, when $\omega = \omega_n$, the transmission and reflection coefficients are:

$$\begin{cases} T_n = T(\omega_n) = \sqrt{\frac{2}{3}} \\ S_{11}(\omega_n) = \sqrt{\frac{7}{15}} \\ S_{22}(\omega_n) = S_{33}(\omega_n) = \sqrt{\frac{1}{15}} \end{cases} \tag{46}$$

We can conclude from these analytical results that the single capacitor three-port circuit shown in Fig. 3 can be classified as a HP-NGD type. The NGD cut-off frequency is given by equation (45).

3.3. NGD optimal frequency

We can demonstrate that our HP-NGD function presents a minimal GD value denoted by:

$$GD_{\min} = \min(GD). \tag{47}$$

Let us denote the optimal angular frequency ω_m. Knowing the expression of GD, we can determine the angular frequency at which we have:

$$GD_{\min} = GD(\omega_m). \tag{48}$$

This frequency is determined by equation:

$$\frac{\partial GD(\omega)}{\partial \omega} = 0. \tag{49}$$

Therefore, we find:

$$\omega_m = \frac{\sqrt{6+5\sqrt{6}}}{3a}. \tag{50}$$

The GD optimal value defined by equation (44) is equal to:

$$GD_{\min} = 3(\frac{2\sqrt{6}}{5} - 1)a \,. \tag{51}$$

Moreover, when $\omega = \omega_m$, the transmission and reflection coefficients are:

$$\begin{cases} T_{\min} = \dfrac{\sqrt{2\sqrt{6}}}{3} \\ S_{11}(\omega_m) = \dfrac{\sqrt{80\sqrt{6} - 135}}{15} \\ S_{22}(\omega_m) = S_{33}(\omega_m) = \dfrac{\sqrt{45 - 10\sqrt{6}}}{15} \end{cases} . \tag{52}$$

3.4. NGD circuit synthesis equation

In this case of study, the synthesis method consists in determining the capacitor in function of the expected specifications of HP-NGD circuit.

3.4.1 Synthesis from cut-off frequency

To get a desired value of cut-off frequency, f_n, the capacitor value can be calculated by inverting equation (45). Therefore, we have:

$$a = \frac{1}{\sqrt{6}\pi f_n} \tag{53}$$

or

$$C = \frac{1}{\sqrt{6}\pi R_0 f_n} \tag{54}$$

3.4.2 Synthesis from GD optimal value

To get a desired value of optimal GD, GD_m, the capacitor value can be calculated by inverting equation (51). Consequently, we have:

$$a = \frac{5GD_{\mathrm{m}}}{3(2\sqrt{6} - 5)} \tag{55}$$

or

$$C = \frac{5GD_{\mathrm{m}}}{3(2\sqrt{6} - 5)R_0} \,. \tag{56}$$

In this case, the optimal frequency versus GD_m is equal to:

$$f_m = \frac{(2\sqrt{6} - 5)\sqrt{6 + 5\sqrt{6}}}{10\pi GD_{\mathrm{m}}} \,. \tag{57}$$

Then, the cut-off frequency versus GD_m is equal to:

$$f_n = \frac{\sqrt{6}(2\sqrt{6}-5)}{10\pi GD_{\mathrm{m}}} \tag{58}$$

In other, we have a linear link between the two frequencies:

$$f_m = \sqrt{1+\frac{5}{\sqrt{6}}}\, f_n \tag{59}$$

3.4.3 Graphical analysis

Fig. 5(a) and Fig. 5(b) plot the variation of capacitor C, optimal and cut-off frequencies, f_m and f_n, versus given optimal GD GD_m. Fig. 5(c) presents the semi-logarithmic plot of the frequencies versus GD_m. The three parameters increase with GD_m. This later one is varied from -10 ns to -1 ns.

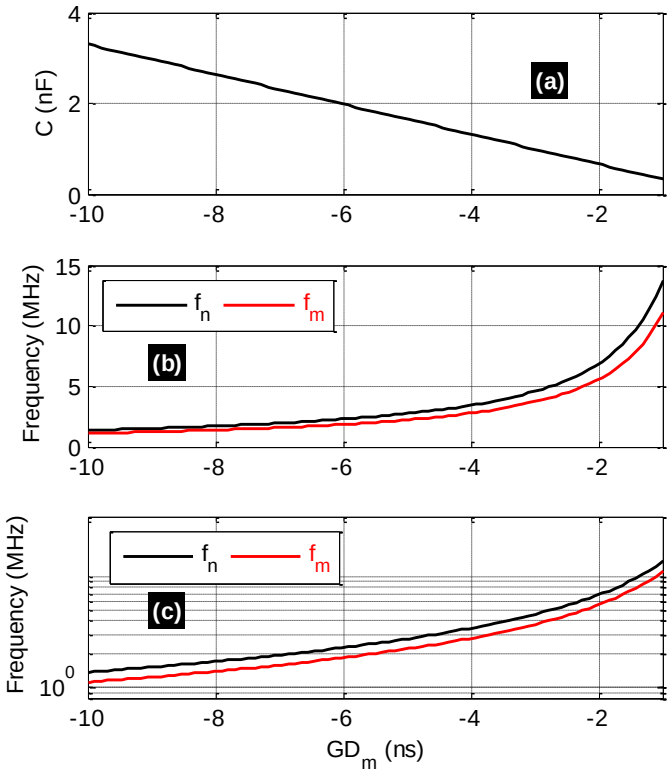

Figure 5: (a) Capacitor, and (b) optimal and cut-off frequencies vs optimal GD.

Table 2 summarizes an example of minimal and maximal values of the synthesized capacitor and frequencies. To validate the developed theory, a proof of concept (POC) of HP-NGD three-port circuit will be studied in the following section.

Parameter	GD_m	C	f_m	f_n

Minimal	-10 ns	0. 33 pF	1.374 MHz	1.11 MHz
Maximal	-1 ns	3.3 pF	13.74 MHz	11.1 MHz

Table 2: Minimal and maximal values of parameters

4. VALIDATION STUDY

The present section is focused on the HP-NGD validation of the theory of single capacitor three-port topology under study. The validation process is based on the comparison of the frequency responses:

- Calculated from MATLAB®,
- Simulation from commercial tool,
- And measurement.

4.1. Design description of single capacitor three-port circuit POC

As POC, a three-port circuit was designed, modeled, simulated and fabricated. Doing this, the design concept is based on the calculation of capacitor in function of the desired GD_m. The capacitor C is determined by relation (56) by taking the series value of GD_m=-0.3 ns, respectively. Thus, the calculated and chosen nominal values of the capacitor are summarized in Table 3.

Description	Parameter	Value
Desired GD	GD_m	-0.3 ns
Calculated value	C	99 pF
Nominal value	C	100 pF

Table 3: Parameters for the single capacitor constituting the designed three-port circuit POC

The design of the single three-port circuit POC was performed from the commercial tool of electronic circuit simulator “Advanced Design System (ADS®)” from Keysight Technologies®. The schematic of the POC circuit designed in the ADS® environment is illustrated by Fig. 6(a). The three-port NGD circuit prototype was fabricated by using a commercial surface mounted device (SMD) capacitor component. The photograph of the fabricated prototype is displayed by Fig. 6(b). Port ① is shown in left and the other access port ② and port ③ are in right side of the printed circuit board by using SMA connectors. Moreover, the three-port circuit prototype was implemented on Cu-metalized FR4 dielectric substrate in hybrid technology. The physical characteristics of the substrate are indicated in Table 4.

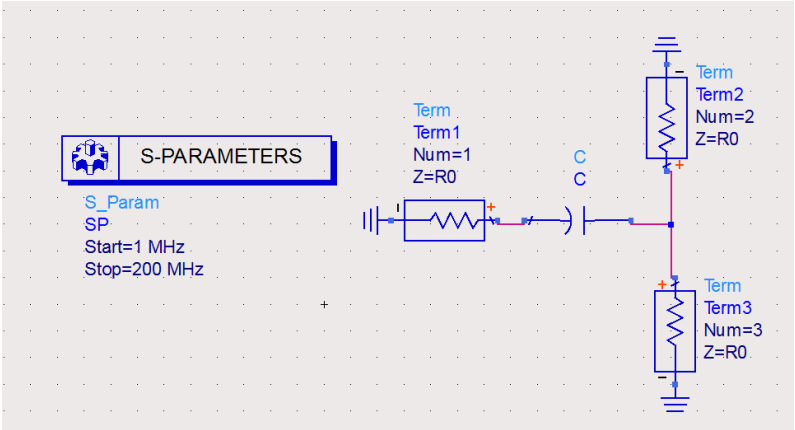

(a)

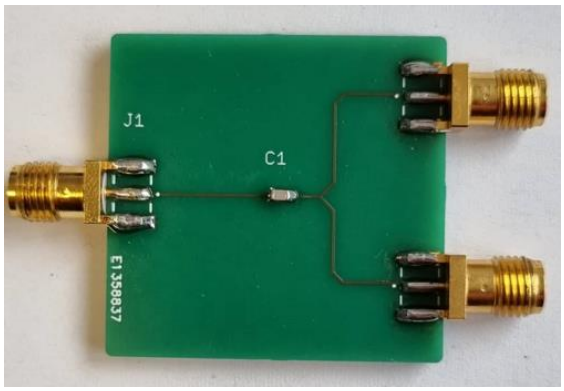

(b)

Figure 6: (a) ADS® design of the simulated and (b) fabricated single capacitor three-port circuit prototype.

Structure	Description	Parameters	Values
Substrate	Relative permittivity	ε_r	4.5
	Loss tangent	$\tan(\delta)$	0.02
	Thickness	h	1.6 mm
Metallization conductor	Copper conductivity	σ	58 MS/m
	Thickness	t	35 µm

Table 4: Physical parameters of the fabricated three-port circuit substrate

4.2 Experimental setup of the single capacitor three-port circuit

Similar to classical microwave circuits, the NGD analysis in the frequency domain is based on three-port S-parameters measurement with a Vector Network Analyzer (VNA) as illustrated by the synoptic diagram of Fig. 7(a).

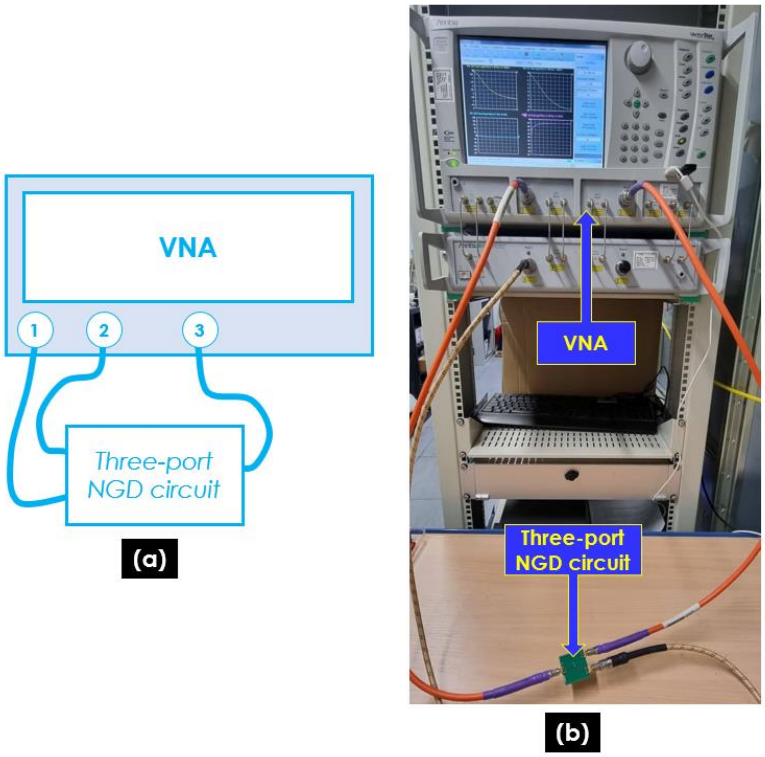

Figure 7: (a) Illustrative diagram and (b) photograph of the three-port HP-NGD circuit prototype experimental setup.

Accordingly, the fabricated three-port circuit prototype, previously introduced in Fig. 7(b), was measured with VNA defined by the manufacturer reference Anritsu MS4647B. The VNA is susceptible to operate the frequency band 70 kHz to 70 GHz. It is noteworthy also that during the measurement process, the S-parameters test was made under Short-Open-Load-Thru (SOLT) calibration. The experimental validation results of the established HP-NGD theory of single capacitor three-port circuit will be elaborated in the following paragraphs.

4.3. Discussion on the validation results

The proposed validation is based on the comparison between the MATLAB® calculation, ADS® simulation and S-parameter measured results. The numerical computation was carried from analytical expressions of:

- Transmission coefficient given in equations (35),
- GD given in equations (37),
- And reflection coefficients given in equations (38) and (39).

4.3.1 Discussion between the calculated and simulated GDs

Fig. 8(a) depicts the comparison of calculated ("Calc.", black solid line), simulated ("Simu.", dashed red line) and measured ("Meas.", dashed blue line) results of GD responses of the designed and tested single capacitor three-port circuit presented in Figs. 7. The GD diagram of Fig. 8(a) is plotted in the wide frequency band from f_{min}=1 MHz and f_{max}=200 MHz. In order to show the NGD aspect, the zoom in plot of the GD responses is additionally displayed in Fig. 8(b).

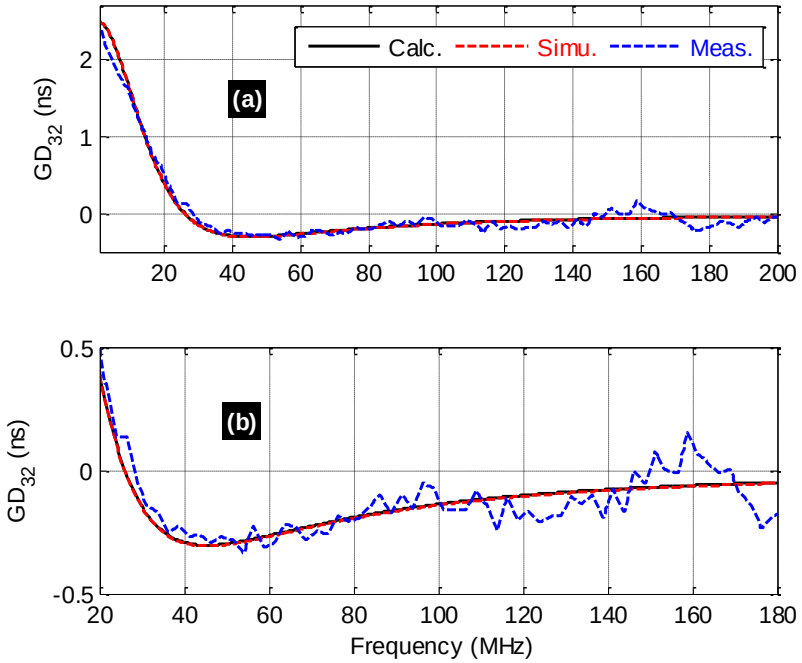

Figure 8: Comparison of calculated and simulated GDs with (a) wideband and (b) narrow band zoom in plots of the three-port circuit shown in Figs. 7.

As expected, we can emphasize a good correlation between the calculated, simulated and tested GDs. The deviation between the measured GDs and the other results at higher frequencies are not due to the modelling method. The differences can be interpreted as follows. The slight difference between the measured and other results is mainly due to:

- the parasitic effect of the employed capacitor,
- the interconnection effects,
- the connector imperfection,
- and also the employed cable imperfections.

More importantly, the GD presents undeniable the HP-NGD behavior with GD having positive values when the frequency is lower than the NGD cut-off frequency of about f_n=37.1 MHz. Then, the GD is negative above f_n. The optimal minimal value of about GD_m=-0.3 ns is reached around the frequency f_m=45.8 MHz.

4.3.2 Discussion between calculated and simulated transmission coefficients

The validation study was also applied to the S-parameters and especially the transmission coefficient magnitude corresponding to the previously discussed GD. Similar to the previous results, the comparison between the calculated, simulated and tested transmission coefficient S_{32} is presented by Figs. 9. The wide band plot is shown by Fig. 9(a). We can underline that there is a good agreement between the calculated, simulated and tested results.

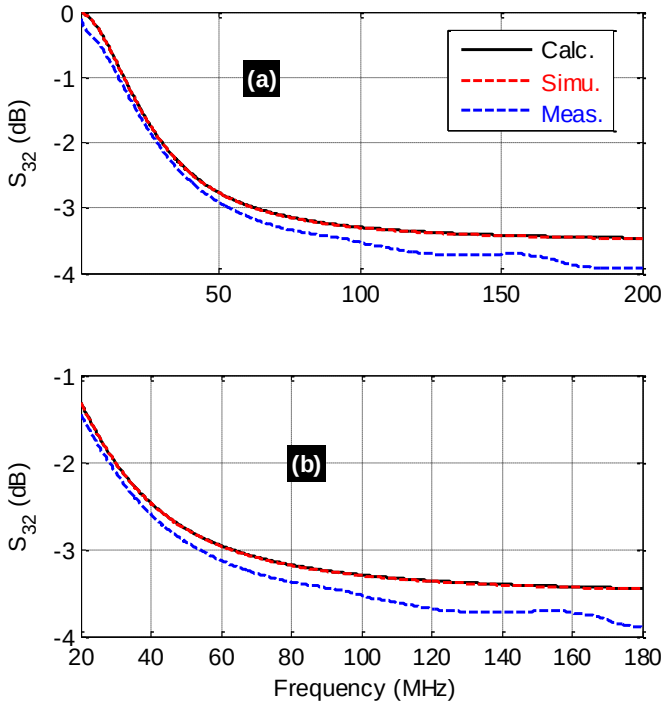

Figure 9: Comparison of calculated and simulated S_{32} in (a) wideband and (b) narrow band zoom in plots of the three-port circuit shown in Figs. 7.

We can see that the transmission coefficient is decreasing when the frequency is increased. These results represent a typical magnitude response of HP-NGD circuit transmission coefficient. The discrepancy of the measured result is mainly due to the parasitic effect of the employed capacitor in the frequency band of the interest.

4.3.3 Discussion between calculated and simulated reflection coefficients

During the validation process, a particular interest was focused on the reflection coefficients of our single capacitor circuit prototype. Fig. 10(a) and Fig. 10(b) display the plots of S_{11} and S_{22} plotted in the wide frequency band from

f_{min}=1 MHz and f_{max}=200 MHz. Once more, there is a good correlation between the calculated, simulated and tested reflection coefficients. In a nutshell, the behaviors of GD, transmission and reflection coefficients of our three-port circuit prototype enable to validate the theoretical model of HP-NGD function between port ② and port ③ .

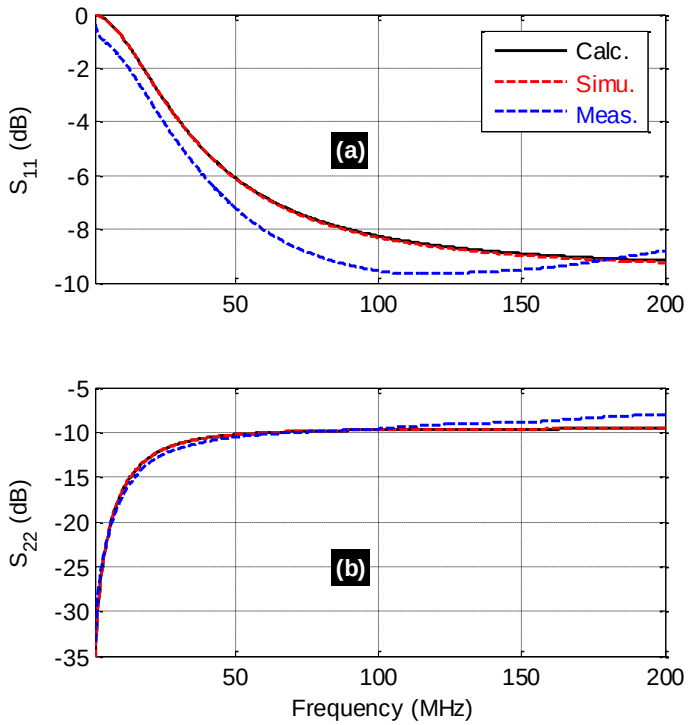

Figure 10: Comparison of calculated and simulated (a) S_{11} and (b) S_{22} of the three-port circuit shown in Figs. 7.

4.4 Discussion on the impact of the present study on the NGD circuit design state of the art

The specific novelty of the HP-NGD circuit topology presented in this paper can be obviously understood with state-of-the-art comparison of NGD topologies available in the literature. Table 5 indicates the essential impact of the proposed study compared to the NGD topology design in [30-43]. In this table, NGD topologies of two- [31-35, 38-39], three- [35-36, 40-41] and four- [42-43] port circuits are discussed. The new contribution of the NGD topology developed in this study is:

- The theory of innovative 3-port HP-NGD topology,
- The S-parameters modelling of single capacitor circuit,
- The design method of 3-port HP-NGD circuit,
- The experimental test methodology of HP-NGD circuit.

References	Nature of components	Number of ports	NGD-type function
[31-32]	RL or RC	2	LP-NGD
[33-34]	RL or RC		HP-NGD
[30]	RLC		BP-NGD
[35,38]	RC		BP-NGD
[38]	RLC		SB-NGD
[39]	RC		SB-NGD
[35]	RLC	3	BP-NGD
[36]	C		BP-NGD
[40]	RC		Double LP- and HP-NGD
[41]	LC		LP-NGD
[42-43]	LC	4	BP-NGD
Proposed work	C	3	HP-NGD

Table 5: State of the art comparison of NGD topology characteristics

5. CONCLUSION

An innovative theory of HP-NGD three-port circuit is studied. The proposed HP-NGD topology is constituted by only a single capacitor. After the topological description, the S-matrix model is established from the Y-matrix by means of KVL and KCL equations.

The HP-NGD analysis is developed from the transmission coefficient and the GD extracted from the transmission phase. It is analytically demonstrated from the identified first order transfer function that the single capacitor three-port circuit is susceptible to behave as a HP-NGD function. The HP-NGD analysis is elaborated by establishing the main NGD characteristics of the considered three-port topology. Then, the synthesis equation allowing to determine the capacitor value in function of the expected NGD optimal value which linked to the NGD cut-off frequency is proposed.

The validity of the HP-NGD theory is theoretically, simulation and experimentally verified. To do this, a POC of single capacitor three-port circuit was designed and simulated with a commercial tool. Then, a prototype with SMD component was fabricated and tested. As expected, simulation and measurement results in very good agreement with the calculated model show the feasibility of the HP-NGD behavior. It was underlined that the parasitic effects and the measurement systematic errors may penalize the HP-NGD circuit responses at higher frequencies. Because of the real component parasitic effects, it was found that the GD response of the HP-NGD circuit prototype may not be always negative above 100 MHz. But such remark does not mean that either the proposed topology or the S-parameter are not valid at higher frequencies.

Despite the progress of the electronic communication system design, considerable challenges remain to overcome as the issue from the signal propagation delay. To face up such issue, the proposed NGD circuit theory, modelling and design can be practically useful in the society for the improvement of performances of many electronic circuits in the future RF/microwave electronic and communication systems through the following original solutions:

- Propagation signal delay compensation [1-2],
- Frequency independent or negligible delay devices as phase shifters and antenna [3-6]
- And communication signal integrity improvement with resonance effect reduction [7-9].

REFERENCES

[1] C. D. Broomfield and J. K. A. Everard, "Broadband Negative Group Delay Networks for Compensation of Oscillators, Filters and Communication Systems," Electron. Lett., Vol. 36, No. 23, pp. 1931-1933, Nov. 2000.

[2] B. Ravelo, S. Lalléchère, A. Thakur, A. Saini and P. Thakur, "Theory and circuit modelling of baseband and modulated signal delay compensations with low- and band-pass NGD effects", Int. J. Electron. Commun., Vol. 70, No. 9, Sept. 2016, pp. 1122–1127.

[3] B. Ravelo, "Distributed NGD active circuit for RF-microwave communication", Int. J. Electron. Commun., Vol. 68, No. 4, Apr. 2014, pp. 282-290.

[4] B. Ravelo, G. Fontgalland, H. S. Silva, J. Nebhen, W. Rahajandraibe, M. Guerin, G. Chan, and F. Wan, "Original Application of Stop-Band Negative Group Delay Microwave Passive Circuit for Two-Step Stair Phase Shifter Designing," IEEE Access, Vol. 10, No. 1, 2022, pp. 1493-1508.

[5] M. Zhu and C.-T. M. Wu, "Reconfigurable Series Feed Network for Squint-free Antenna Beamforming Using Distributed Amplifier-Based Negative Group Delay Circuit," in Proc. 2019 49th European Microwave Conference (EuMC), Paris, France, 1-3 Oct. 2019, pp. 256-259.

[6] B., Ravelo, W., Rahajandraibe, Y., Gan, F., Wan, N. M., Murad and A. Douyère, "Reconstruction Technique of Distorted Sensor Signals with Low-Pass NGD Function," IEEE Access, vol. 8, no. 1, pp. 92182-92195, 2020.

[7] B. Ravelo, F. Wan, J. Nebhen, W. Rahajandraibe, and S. Lalléchère, "Resonance Effect Reduction with Bandpass Negative Group Delay Fully Passive Function," IEEE Transactions on Circuits and Systems II: Express Briefs, Vol. 68, No. 7, July 2021, pp. 2364-2368.

[8] B. Ravelo, S. Lalléchère, W. Rahajandraibe, and F. Wan, "Electromagnetic Cavity Resonance Equalization with Bandpass Negative Group Delay," IEEE Transactions on Electromagnetic Compatibility, Vol. 63, No. 4, Aug. 2021, pp. 1248-1257.

[9] S. Chu and S. Wong, "Linear Pulse Propagation in an Absorbing Medium," Phys. Rev. Lett., Vol. 48, 1982, pp. 738-741.

[10] B. Ségard and B. Macke, "Observation of Negative Velocity Pulse Propagation," Phys. Lett. A, Vol. 109, 1985, pp. 213-216.

[11] J. N. Munday and W. M. Robertson, “Observation of Negative Group Delays within a Coaxial Photonic Crystal Using an Impulse Response Method,” Optics Communications, Vol. 273, No. 1, 2007, pp. 32-36.

[12] B. Ségard and B. Macke, “Two-pulse interference and superluminality,” Optics Communications, Vol. 281, No. Jan. 2008, pp. 12–17.

[13] M. W. Mitchell, and R. Y. Chiao, “Negative group delay and "fronts" in a causal system: An experiment with very low frequency bandpass amplifiers,” Phys. Lett. A, vol. 230, no. 3-4, June 1997, pp. 133-138.

[14] M. W. Mitchell and R.Y. Chiao, “Causality and Negative Group-delays in a Simple Bandpass Amplifier,” Am. J. Phys., vol. 66, 1998, pp. 14-19.

[15] T. Nakanishi, K. Sugiyama and M. Kitano, “Demonstration of Negative Group-delays in a Simple Electronic Circuit,” Am. J. Phys., vol. 70, no. 11, 2002, pp. 1117-1121.

[16] M. Kitano, T. Nakanishi and K. Sugiyama, “Negative Group-delay and Superluminal Propagation: An Electronic Circuit Approach,” IEEE J. Sel. Top. in Quantum Electron., vol. 9, no. 1, Feb. 2003, pp. 43-51.

[17] J. N. Munday and R. H. Henderson, “Superluminal Time Advance of a Complex Audio Signal,” Appl. Phys. Lett., vol. 85, no. 3, July 2004, pp. 503-504.

[18] G. V. Eleftheriades, O. Siddiqui, and A. K. Iyer, “Transmission Line for Negative Refractive Index Media and Associated Implementations without Excess Resonators,” IEEE Microw. Wireless Compon. Lett., Vol. 13, No. 2, pp. 51-53, Feb. 2003.

[19] O. F. Siddiqui, M. Mojahedi and G. V. Eleftheriades, “Periodically Loaded Transmission Line With Effective Negative Refractive Index and Negative Group Velocity,” IEEE Trans. Antennas Propagat., Vol. 51, No. 10, Oct. 2003, pp. 2619-2625.

[20] L. Markley and G. V. Eleftheriades, “Quad-Band Negative-Refractive-Index Transmission-Line Unit Cell with Reduced Group Delay,” Electronics Letters, Vol. 46, No. 17, Aug. 2010, pp. 1206-1208.

[21] G. Monti and L. Tarricone, “Negative Group Velocity in a Split Ring Resonator-Coupled Microstrip Line,” Progress In Electromagnetics Research, Vol. 94, pp. 33-47, 2009.

[22] G. Liu, and J. Xu, “Compact transmission-type negative group delay circuit with low attenuation,” Electronics Letters, Vol. 53, No. 7, Mar. 2017, pp. 476-478.

[23] G. Chaudhary, and Y. Jeong, “Tunable center frequency negative group delay filter using coupling matrix approach,” IEEE Microwave Wireless Component Letters, Vol. 27, No. 1, 2017, pp. 37-39.

[24] T. Shao, S. Fang, Z. Wang and H. Liu, “A Compact Dual-Band Negative Group Delay Microwave Circuit,” Radio Engineering, vol. 27, no. 4, pp. 1070-1076, Dec. 2018.

[25] M. Kandic and G. E. Bridges, “Asymptotic Limits of Negative Group Delay in Active Resonator-Based Distributed Circuits,” IEEE Transactions on Circuits and Systems I: Regular Papers, Vol. 58, No. 8, Aug. 2011, pp. 1727-1735.

[26] C.-T. M. Wu and T. Itoh, “Maximally Flat Negative Group Delay Circuit: A Microwave Transversal Filter Approach,” IEEE Trans. on Microwave Theory and Techniques, Vol. 62, No. 6, June 2014, pp. 1330-1342.

[27] T. Zhang, R. Xu and C. M. Wu, “Unconditionally Stable Non-Foster Element Using Active Transversal-Filter-Based Negative Group Delay Circuit,” IEEE Microw. Wireless Compon. Lett., vol. 27, no. 10, pp. 921-923, Oct. 2017.

[28] B. Ravelo, “Similitude between the NGD function and filter gain behaviours,” Int. J. Circ. Theor. Appl., Vol. 42, No. 10, Oct. 2014, pp. 1016-1032.

[29] B. Ravelo, “On the low-pass, high-pass, bandpass and stop-band NGD RF passive circuits”, URSI Radio Science Bulletin, Vol. 2017, No. 363, Dec. 2017, pp. 10-27.

[30] B. Ravelo, “First-order low-pass negative group delay passive topology”, Electronics Letters, Vol. 52, No. 2, Jan. 2016, pp. 124–126.

[31] R. Randriatsiferana, Y. Gan, F. Wan, W. Rahajandraibe, R. Vauché, N. M. Murad and B. Ravelo, “Study and Experimentation of a 6-dB Attenuation Low-Pass NGD Circuit,” Analog. Integr. Circ. Sig. Process., pp. 1-14, Apr. 2021.

[32] F. Wan, X. Huang, K. Gorshkov, B. Tishchuk, X. Hu, G. Chan, F. E. Sahoa, S. Baccar, M. Guerin, W. Rahajandraibe and B. Ravelo, “High-pass NGD characterization of resistive-inductive network based low-frequency circuit,” COMPEL - The International Journal for Computation and Mathematics in Electrical and Electronic Engineering, Vol. 40, No. 5, pp. 1032-1049, 2021.

[33] R. Yang, X. Zhou, S. Yazdani, E. Sambatra, F. Wan, S. Lalléchère and B. Ravelo, “Analysis, design and experimentation of high-pass negative group delay lumped circuit”, Circuit World, Aug. 2021, pp. 1-25.

[34] B. Ravelo, S. Ngoho, G. Fontgalland, L. Rajaoarisoa, W. Rahajandraibe, R. Vauché, Z. Xu, F. Wan, J. Ge, and S. Lalléchère, “Original Theory of NGD Low Pass-High Pass Composite Function for Designing Inductorless BP NGD Lumped Circuit,” IEEE Access, Vol. 8, No. 1, Oct. 2020, pp. 192951-192964.

[35] J. Nebhen and B. Ravelo, “Bandpass NGD analysis of symmetric lumped Y-tree via tensorial analysis of networks formalism,” Journal of Electromagnetic Waves and Applications, Vol. 35, No. 16, 2021, pp. 2125-2140.

[36] F. Wan, Y. Liu, J. Nebhen, Z. Xu, G. Chan, S. Lalléchère, R. Vauche, W. Rahajandraibe and B. Ravelo, “Bandpass Negative Group Delay Theory of Fully Capacitive Δ-Network,” IEEE Access, Vol. 9, No. 1, pp. 62430 - 62445, Apr. 2021.

[37] S. Lalléchère, J. Nebhen, Y. Liu, G. Chan, G. Fontgalland, W. Rahajandraibe, F. Wan and B. Ravelo, “Suitability of passive RC-network-based inductorless bridged-T as a bandpass NGD circuit”, Circuit World, Nov. 2021, pp. 1-15.

[38] S. Fenni, F. Haddad, K. Gorshkov, B. Tishchuk, A. Jaomiary, F. Marty, G. Chan, M. Guerin, W. Rahajandraibe and B. Ravelo, “AC low-frequency characterization of stop-band negative group delay circuit,” Progress In Electromagnetics Research (PIER) C, Vol. 115, pp. 261-276, 2021.

[39] M. Guerin, Y. Liu, A. Douyère, G. Chan, F. Wan, S. Lalléchère, W.Rahajandraibe, and B. Ravelo, “Design and Synthesis of Inductorless Passive Cell Operating as Stop-Band Negative Group Delay Function,” IEEE Access, Vol. 9, No. 1, July 2021, pp. 100141–100153.

[40] H. Jia, F. Wan, J. Frnda, M. Guerin, W. Rahajandraibe, P. Thakur, A. Thakur, B. Agnus and B. Ravelo, “Novel Tee-Shaped Topology Theory of Low- and High-Pass NGD Double-Type Function,” IEEE Access, Vol. 10, No. 1, 2022, pp. 28445 - 28460.

[41] E. J. R. Sambatra, A. Jaomiary, S. Ngoho, S. S. Yazdani, N. M. Murad, G. Chan and B. Ravelo, “Low-pass negative group delay modelling and experimentation with tri-port resistorless passive cross-circuit,” Progress In Electromagnetics Research (PIER) M, Vol. 108, pp. 39-51, 2022.

[42] B. Ravelo, F. Wan, J. Nebhen, G. Chan, W. Rahajandraibe and S. Lalléchère, “Bandpass NGD TAN of Symmetric H-Tree with Resistorless Lumped-Network,” IEEE Access, Vol. 9, pp. 41383-41396, Mar. 2021.

[43] B. Ravelo, J. Nebhen, M. Guerin, G. Chan and W. Rahajandraibe, “Tensorial-analysis-of-networks applied to bandpass negative-group-delay analysis of resistorless LC-coupler-network,” Radio Science, Vol. 57, No. 4, pp. 1-13, Apr. 2022.